Supplementary Information (SI)

Section 1: Assessing the accuracy of NEA recordings when compared to patch clamp

Ensuring the accuracy of the training data is vital for the effectiveness of any deep learning model. To determine the accuracy of iAP waveforms obtained from NEAs, we performed simultaneous NEA and patch clamp recording from the same cell and compared various features of their waveforms. Nano Crown-shaped NEAs (referred to simply as NEAs herein) were fabricated as previously reported [1]. iPSC-CM cells were then seeded onto the NEAs employing a differentiation and culture protocol as outlined in the Methods section.

We performed 15 sets of simultaneous iAP recordings from single cells, utilizing both patch clamp and NEA methods, with a comparative analysis of their waveforms shown in Figure-SI-1a. Each recording set, as depicted in Figure-SI-1b, demonstrated that although NEA iAP traces exhibit a lower amplitude, they closely align with the patch-clamp recordings when normalized. This normalization process allowed for a more accurate comparison between the two techniques. The total duration of these simultaneous recordings was approximately 46 minutes. To quantify the similarity between waveforms, we initially applied high-pass and low-pass filtering, as detailed in the Methods section, to decompose the waveform into isolated noise and refined action potential waveform. To account for various iAP shapes collected during recording, the signals were then segregated using a window length of 8000 timepoints or 1.6 seconds.

This process yielded a total of 3363 pairs of iAP recordings from both NEA and patch clamp methods. The S/N for both NEA and patch recordings was calculated by utilizing the filtered signal and noise vectors, assigning an S/N value to each window of the respective recording methods. Each window, containing pairs of action potential signals, was then normalized to a scale ranging from 0 to 1 to facilitate a more precise comparison. Furthermore, we quantified the APD values and their differences within each window, along with the cycle time for each recording (Figure-SI-1c). We also calculated the discrepancy in cycle times between the NEA and patch clamp methods. Additionally, we determined the Mean Absolute Error (MAE) and analyzed the correlation (r) within each window (Figure-SI-1d). This comprehensive analysis, which included comparisons of NEA and patch clamp recordings as depicted in the Figure-SI-1, provided an in-depth evaluation of the compatibility between these two recording techniques.

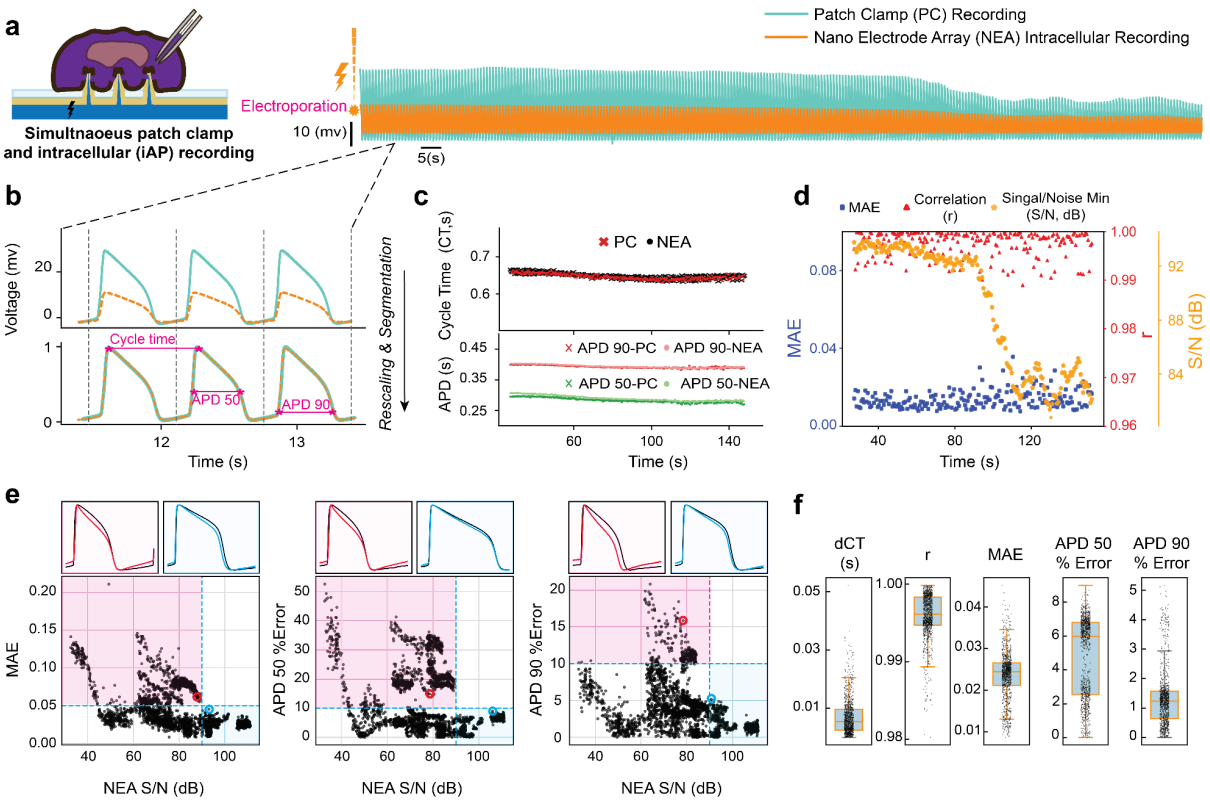

Figure-SI-1. a) Simultaneous iAP recording from iPSC-CMs using patch clamp (PC) and nano electrode array (NEA) via electroporation. **b)** Comparison of iAP recordings from PC and NEA: Scaling between 0 to 1 and segmenting into arrays of length 8000 indices or 1.6s. Includes important features such as cycle time, APD50 (action potential duration at 50% repolarization), and APD90. **c)** Comparison between windows of iAP from PC and NEA by cycle time, APD50, and APD90. **d)** Illustration of mean absolute error (MAE), correlation coefficient (r), and NEA signal to noise ratio (S/N) changes over time during one set of the experiment. **e)** Comparison between MAE, APD50% error, and APD90% error vs NEA S/N. It highlights the changes in three critical errors describing the similarity of NEA-recorded and PC-recorded normalized iAPs (MAE, APD50 percentage error, and APD90 percentage error), with thresholds set at 0.05, 10%, and 10% respectively to ensure reasonable similarity between iAP pairs. Also included is the comparison between iAP pairs with the highest MAE with NEA S/N > S/N threshold (S/N*), shown in blue, as well as examples of iAP pairs with error exceeding the threshold from the region with NEA S/N < 90. **f)** Box plot distribution of cycle time difference (dCT(s), r, MAE, APD50%, and APD90% errors between PC and NEA normalized iAP pairs with NEA S/N > S/N* (= 90).

The measured low MAE of 0.046 ±0.028 and a high average correlation (r) of 0.989 ± 0.012 pointed to the near-perfect agreement between the NEA iAP and patch-clamp recordings. Further, key parameters linked to drug-induced heart rhythm abnormalities were investigated by assessing iAP measurements from NEAs against patch clamping, focusing on APD50, and APD90 (cell repolarization markers) and cycle time . The average errors for APD50, and APD90 between NEA iAPs and patch clamps during the experiment were 0.032±0.034(s), and 0.011±0.016(s), respectively. Expressed as percentage errors, these values equate to 11.516±10.010%, and 3.875±3.425%, respectively. For cycle time, the mean difference between two consecutive spikes was 0.011 ± 0.024 (s). Figure-SI-1e illustrates how the MAE, APD 50, and APD 90 errors vary across a range of values depending on the S/N in NEA recording traces.

The figure highlights that as the NEA S/N ratio increases, the maximum values of these errors decrease. This trend suggests that low S/N ratios may cause distortions in iAP shape, potentially due to an imperfect cell-to-NEA seal[1]. These distortions seem to follow a probability distribution dependent on the S/N value, with deviations diminishing at higher S/N ratios. Based on these findings, to ensure waveform accuracy, we set maximum acceptable thresholds at 0.05 for MAE, and 10% for both APD 50 and APD 90

percentage errors. Our analysis revealed that applying a stringent threshold of 90 dB (S/N* =90 dB) and filtering signals with S/N ratios above S/N* ensured that the APD 50 percentage error and MAE remained below 10% and 0.1, respectively, as demonstrated in Figure-SI-1e. The figure also presents examples of eAP and iAP pairs that illustrate the maximum errors observed at or above the S/N*.

Upon comparing NEA iAPs that satisfied the S/N* with corresponding patch clamp iAP recordings, we observed a significant reduction in errors. MAE decreased to 0.024±0.006, and the average correlation coefficient (r) increased to 0.996 ± 0.003. The average errors for APD50 and APD90 between NEA iAPs and patch clamps improved to 0.017±0.020 seconds and 0.004±0.007 seconds, respectively. When expressed as percentage errors, these values correspond to 4.815±2.342% for APD50 and 1.343±0.993% for APD90. Additionally, the mean cycle time difference between two consecutive spikes was recorded at 0.007 ± 0.006 seconds. The distributions of aforementioned errors are shown in Figure-SI-1f. Furthermore, the experiment level comparison of normalized iAPs from NEA recording and patch clamp is provided in Figure-SI-2. These findings align with a comprehensive comparison of NEA and patch clamp iAPs, particularly when various drugs were introduced during recordings [1]. Our findings revealed a near-perfect match between iAPs from the two recording methods when the S/N* was exceeded. We used this S/N* threshold for processing of data used to train our model in subsequent steps.

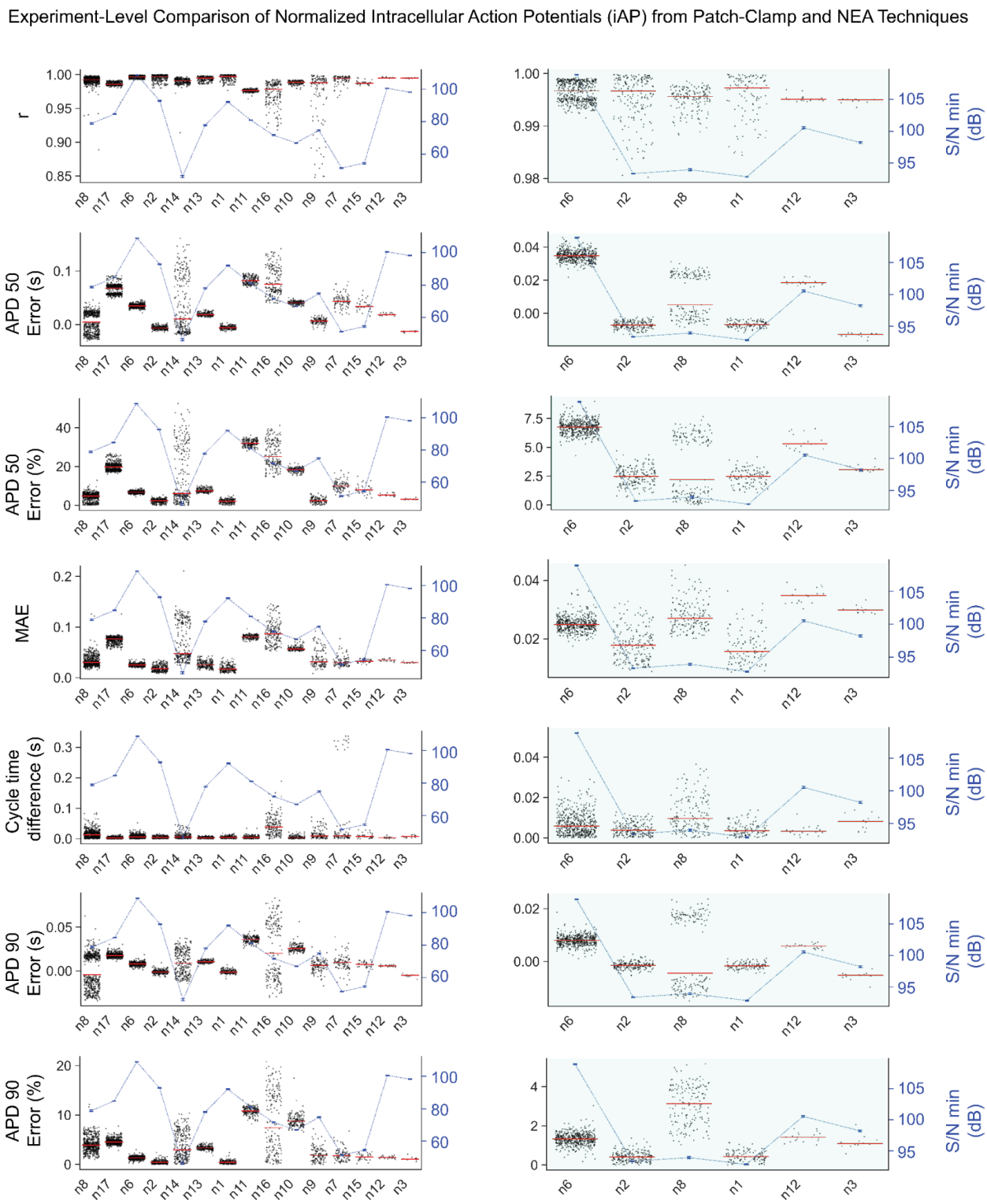

Figure-SI-2. **Experiment-level comparison of normalized iAP from patch clamp (PC) and nano-electrode array (NEA) recording techniques.** Fifteen unique sets of successfully simultaneous iAP recordings using NEA and PC are presented, showcasing various errors (r, APD 50, APD 90, MAE, cycle time difference, APD 50%, and APD 90%). The left panel displays comparisons for all recordings, while the right panel focuses on recordings with NEA iAP signal-to-noise ratio (S/N) greater than 90 and comprising more than 10 samples.

Section II: *Two neighboring channels on NEA show similar iAPs.*

To obtain synchronized eAP and iAP recordings from NEAs, we assumed that neighboring cells in a confluent monolayer of iPSC-CMs that are in close physical proximity on the NEAs exhibit similar AP waveform. We tested this assumption by thoroughly assessing the similarity between neighboring channels over an extended period of time, and under various conditions (Figure-SI-3). To this end, we incrementally introduced Dofetilide (dissolved in DMSO) – a compound known to prolong iAP duration [2] – into the cell culture while recording iAP signals from many channels. The drug's concentration was progressively increased from 0.3 to 1, then to 3, and finally to 10 nM through a multi step addition process. This process was done in four stages, occurring approximately at 400, 800, 1200, and 1700 seconds during the recording session, as illustrated in Figure-SI-3a. Dofetilide addition enables us to study the similarity between two neighboring channels for a wider range of iAP durations. In total, 2661 pairs for iAP spikes from 22 pairs of simultaneous recordings from neighboring channels were collected with S/N > 90 (dB). We applied the same similarity analysis we conducted for NEA versus patch clamp iAPs. We scaled paired NEA neighboring channels iAPs to a range of 0 to 1 (Figure-SI-3b), then calculated the MAE, and correlation between them along with comparing their APD 50, APD 90 and cycle time (Figure-SI-3c). The average difference (MAE) across two iAP traces was 0.011 ± 0.006. Moreover, the correlation coefficients (r) between the iAPs two neighboring channels were quantified as 0.999 ± 0.001 respectively. The average errors for APD50, and APD90 between two neighboring NEA channels iAPs were 0.015±0.009(s), and 0.006±0.005(s), respectively. Expressed as percentage errors, these values equate to 3.943±2.233%, and 3.943±2.233 %, respectively. For cycle time, the mean difference between two consecutive spikes was 0.002±0.002 (s).

Moreover, Figure-SI-3d exhibits pairs of iAPs from neighboring channels, highlighting the maximum MAE, APD 50 percentage error, and APD 90 percentage error observed. This evidence underscores the consistency in iAP traces from neighboring NEA channels when the S/N ratio is greater than the S/N*. This noteworthy outcome underscores the potential to use two neighboring channels to record synchronously from two adjacent cells in a confluent monolayer effectively obtaining both eAP from one channel and iAP from the other, as if acquiring both from a single cell. Leveraging this understanding, in the next step, we electroporated a cell through one channel while recording eAP from the adjacent cell, enabling the simultaneous capture of both eAP and iAP data. This approach was implemented to record the input (eAP) and corresponding output (iAP) data of our data analysis, machine learning, and deep learning models.

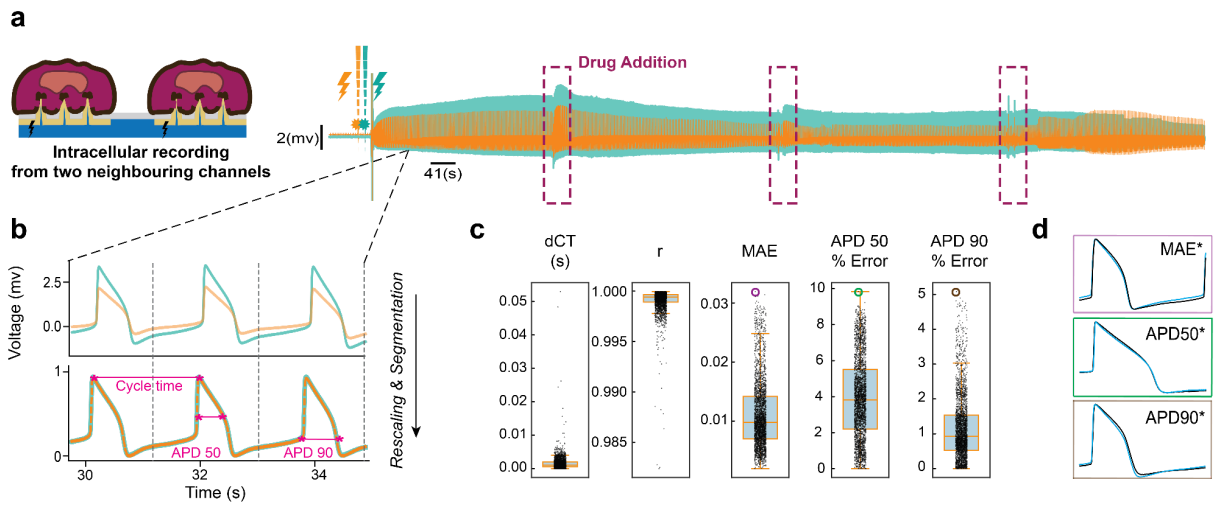

Figure-SI-3. ***a)*** *Simultaneous iAP recording from neighboring channels via non-invasive extracellular action potential (NEA) electroporation. This section details the multi-step addition process of Dofetilide, administered in concentrations of 0.3, 1, 3, and finally 10 nM. The process was conducted in four stages at approximately 400, 800, 1200, and 1700 seconds during the recording session. This method was employed to collect a diverse range of iAP shapes, facilitating a more comprehensive analysis.* ***b)*** *Comparison process similar to PC vs NEA iAP recording: Scaling between 0 to 1 and segmenting into arrays of length 8000 indices or 1.6s.* ***c)*** *Box plot distribution of dCT(s), correlation coefficient (r), MEA, and APD50% and APD90% errors between neighboring and NEA normalized iAP pairs with NEA S/N > S/N* (= 90).* ***d)*** *Examples of iAP pairs from neighboring channels with the highest MEA, APD50, and APD90% errors, as indicated in the box plots.*

The experiment-level comparison of normalized iAPs from neighboring NEA channels is shown in Figure-SI-4.

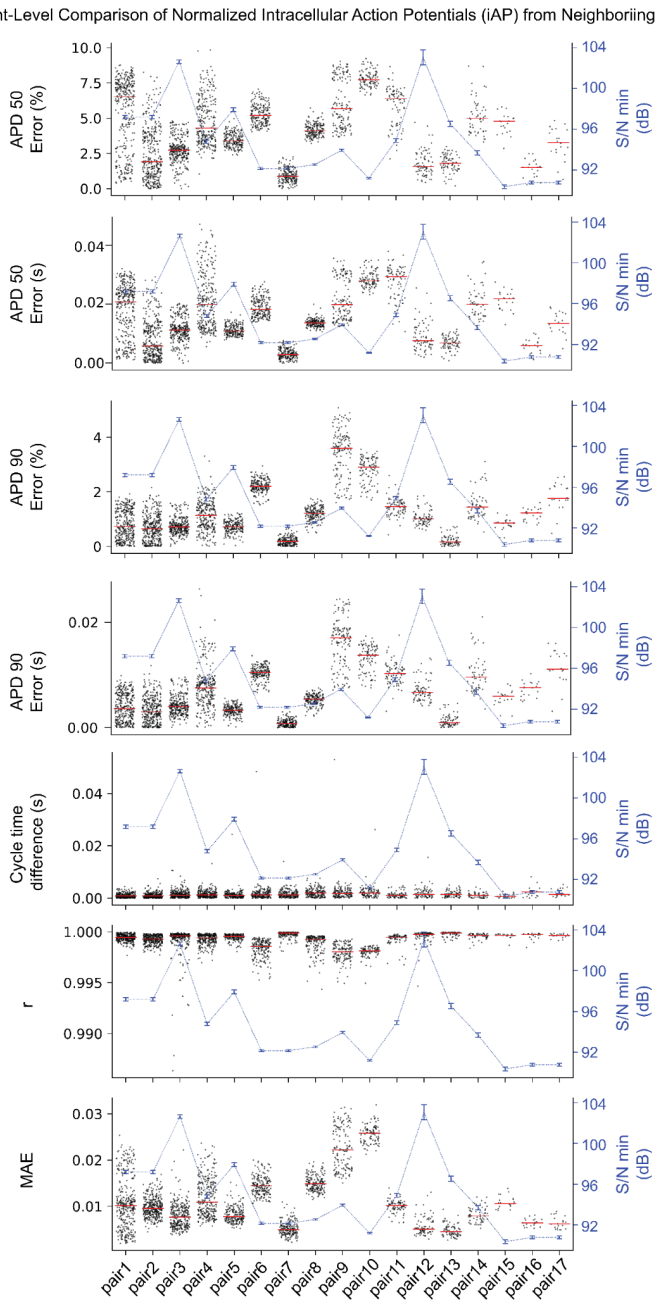

Figure-SI-4. **Experiment-level comparison of normalized iAPs from neighboring NEA channels with a minimum S/N > 90**, involving 17 pairs of channels recorded in two distinct experiments. This comparison highlights various errors, including correlation coefficient (r), APD 50, APD 90, mean absolute error (MAE), cycle time difference, and percentage errors for APD 50% and APD 90%.

Section III: *eAP features screening.*

Distorted spikes in eAP signals, as shown in Figure 2b, and the strong correlation between ΔT_1 and ΔT_2 with ΔT_s (r = 0.83 and r = 0.92, respectively), led us to opt ΔT_s the representative of the eap spike temporal features. Additionally, as shown in Figure-SI-5, the high correlation between DR and ΔV_d (r = 0.97) justified using DR as the sole representative for both in our model. These integrations preserve data integrity and retain crucial eAP waveform information for modeling.

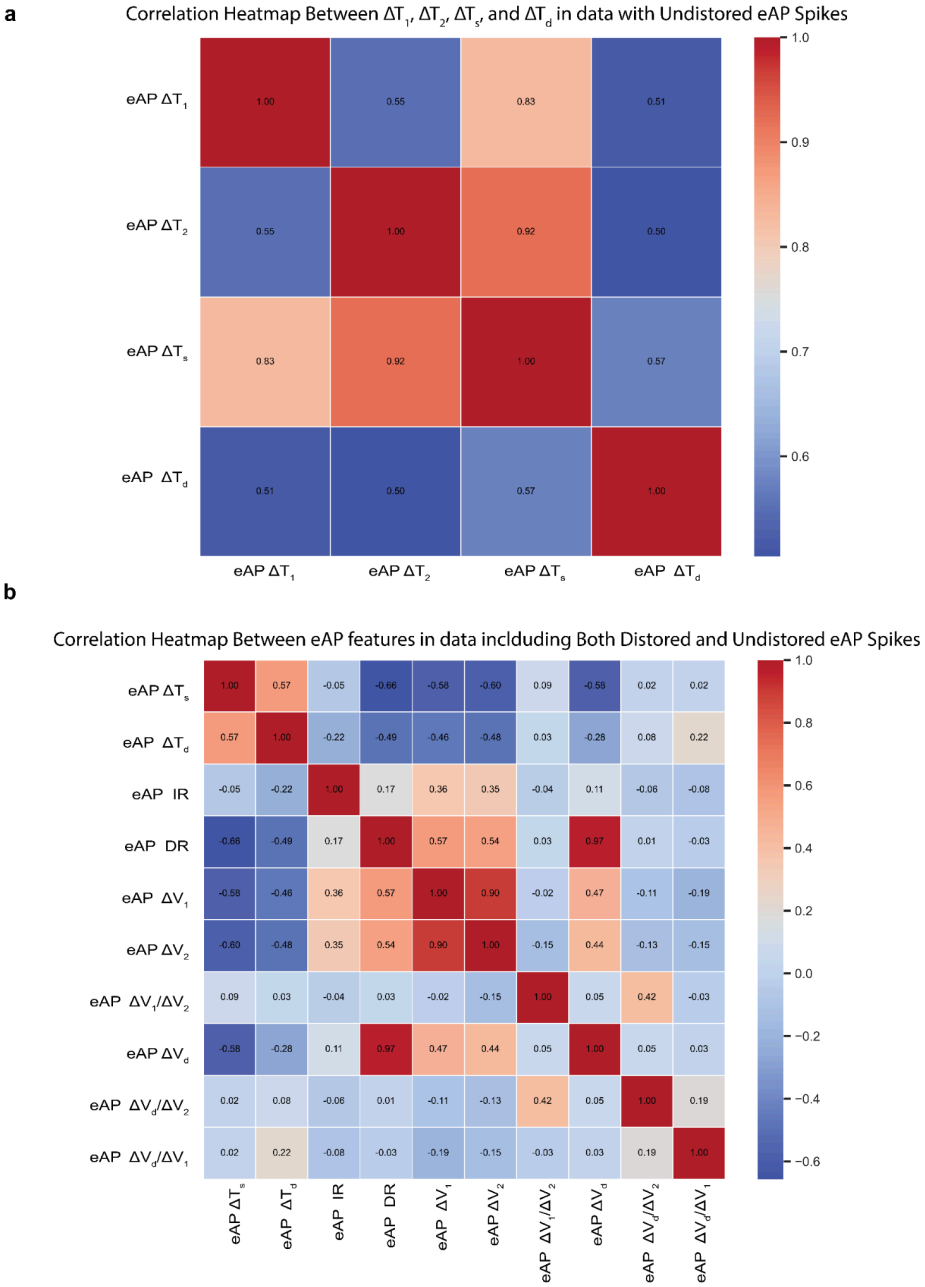

Figure-SI-5. ***a)*** *Correlation between temporal-related eAP features (*ΔT_1*,* ΔT_2*,* ΔT_s*, and* ΔT_d***)*** *for the undistorted portion of eAP/iAP data collected to be utilized in the machine learning and deep learning models.* ***b)*** *Correlation between measurable eAP features (* *excluding* ΔT_1 *and* ΔT_2***)*** *for all of the eAP/iAP data (with distorted and undistorted eap spikes) utilized in the machine learning and deep learning models.*

Section IV: *Baseline Models.*
During our experimentation, we employed various models, namely LTSF-Linear, LTSF-DLinear, LTSF-NLinear, and Multilayer Perceptron, as baselines to predict iAP from eAP.

LTSF-Linear

LTSF-Linear, proposed in [3], is a type of one-layer linear model that directly forecasts future time series by regressing historical time series. Despite having a simple design, it outperforms transformer-based models for the task of long-term time series forecasting. This raises questions about the effectiveness of transformers for this task, and for this reason, we included LTSF-Linear in our work to validate the accuracy of Unet.

The basic formulation of LTSF-Linear involves directly regressing historical time series to forecast future time series using a weighted sum operation. Specifically, it uses L historical timesteps to predict *T* future timesteps, with the mathematical expression being $\hat{X}_{i+1:i+T} = W X_{i-L:i}$, where $W \in R^{T \times L}$ is a linear layer along the temporal axis. $\hat{X}_i$ and X_i are the prediction and input for each variable, respectively. It is important to note that LTSF-Linear shares weights across different variates and does not model any spatial correlations. Although originally used for long-term time series forecasting, we adapted it for the eAP-iAP prediction task in our study.

Apart from the basic formulation, there are two other variants of LTSF-Linear described in [1]: DLinear and NLinear. DLinear combines a decomposition scheme that decomposes a raw data input into a trend component using a moving average kernel and a remainder (seasonal) component. It then applies two one-layer linear layers to each component and sums them up to obtain the final prediction. This variant improves the performance of a vanilla linear layer when there is a clear trend in the data. NLinear, on the other hand, further enhances the performance of LTSF-Linear when there is a distribution shift in the dataset. It first subtracts the input by the last value of the sequence and then applies a linear layer to the input. Finally, it adds back the subtracted part to generate the final prediction. The subtraction and addition operations in NLinear normalize the input sequence.

In the original paper [3], the model predicted the output sequence directly from the input sequence. However, adopting the same approach for eAP-iAP prediction would result in a large number of parameters (8000 x 8000), leading to suboptimal results. To address this issue, we modified the architecture by applying average pooling on the 8000-sized eAP input to obtain a low-dimensional vector (of size N). We then used unpooling on the low-dimensional vector to obtain the 8000-sized iAP output. This modification reduces the number of trainable parameters to 2xNx8000, leading to better results.

LTSF-Linear
Input (8000)
FC (N units)
FC (8000)

LTSF-DLinear
Input (8000)
Series Decomposition (Trend + Seasonal)
FC (N units)
FC (8000) (Trend + Seasonal)

LTSF-NLinear
Input (8000)
Input - last value in sequence (8000)
FC (N units)
FC (8000)

Multilayer Perceptron

A Multilayer Perceptron (MLP) is a type of artificial neural network used for supervised learning. It consists of multiple layers of fully connected nodes, where each node represents a mathematical function that takes input from the previous layer and produces an output that is sent to the next layer. The input layer of an MLP accepts input data, which is then passed through a series of hidden layers, each of which performs a nonlinear transformation of the input. The output of the final hidden layer is then fed into the output layer, which produces the final output of the network. MLPs have been used for prognosis prediction[4], analyzing cancer sequencing data [5], analyzing RNA sequencing [6], and predicting protein-ligand binding affinity [7].

The motivation behind using an MLP for this task is its ability to model complex non-linear relationships in data. Sequences often exhibit patterns that may not be captured effectively by linear models. Also, MLPs can capture information from past elements in a sequence, making them suitable for tasks where predicting the next element depends on a combination of current and past elements.

MLP architecture
Input - 8000
FC - N1 + ReLU
FC - N2 + ReLU
FC - N3 + ReLU
FC - 8000

As shown in the table above, we trained an MLP to predict 8000 timesteps of iAP from 8000 timesteps of eAP. This model has L hidden layers, each with some hidden units. A ReLU activation function is applied after every linear layer for introducing non-linearity.

Training details

All the models above were trained on the dataset with 8000 timesteps.

1. Contains 1910 pairs of eAP-iAP recordings
2. Training set → 1248 eAP-iAP pairs (from first 2 sets of experiments)
3. Validation set → 313 eAP-iAP pairs (from first 2 sets of experiments)
4. Test set → 349 eAP-iAP pairs (from third experiment set)

Adam optimizer was used for optimizing the models and MSE was used as the loss function.

References

1. Jahed, Z. *et al.* Nanocrown electrodes for parallel and robust intracellular recording of cardiomyocytes. *Nat. Commun.* **13**, 2253 (2022).
2. Marschang, H., Beyer, T., Karolyi, L., Kübler, W. & Brachmann, J. Differential rate and potassium-dependent effects of the class III agents d-sotalol and dofetilide on guinea pig papillary muscle. *Cardiovasc. Drugs Ther.* **12**, 573–583 (1998).
3. Zeng, A., Chen, M., Zhang, L. & Xu, Q. Are Transformers Effective for Time Series Forecasting? *AAAI* **37**, 11121–11128 (2023).

4. Ching, T., Zhu, X. & Garmire, L. X. Cox-nnet: An artificial neural network method for prognosis prediction of high-throughput omics data. *PLoS Comput. Biol.* **14**, e1006076 (2018).
5. Ainscough, B. J. *et al.* A deep learning approach to automate refinement of somatic variant calling from cancer sequencing data. *Nat. Genet.* **50**, 1735–1743 (2018).
6. Brendel, M. *et al.* Application of Deep Learning on Single-cell RNA Sequencing Data Analysis: A Review. *Genomics Proteomics Bioinformatics* **20**, 814–835 (2022).
7. Yin, Z. *et al.* Neural networks prediction of the protein-ligand binding affinity with circular fingerprints. *Technol. Health Care* **31**, 487–495 (2023).